

Photovoltaic Hot-Spot Detection for Solar Panel Substrings Using AC Parameter Characterization

Katherine A. Kim, *Member, IEEE*, Gab-Su Seo, *Student Member, IEEE*, Bo-Hyung Cho, *Fellow, IEEE*, and Philip T. Krein, *Fellow, IEEE*

Abstract—Hot spotting is a problem in photovoltaic (PV) systems that reduces panel power performance and accelerates cell degradation. In present day systems, bypass diodes are used to mitigate hot spotting, but it does not prevent hot spotting or the damage it causes. This paper presents an active hot-spot detection method to detect hot spotting within a series of PV cells, using ac parameter characterization. A PV cell is comprised of series and parallel resistances and parallel capacitance, which are affected by voltage bias, illumination, and temperature. Experimental results have shown that when a PV string is under a maximum power point tracking control, hot spotting in a single cell results in a capacitance increase and dc impedance increase. The capacitance change is detectable by measuring the ac impedance magnitude in the 10–70 kHz frequency range. An impedance value change due to hot spotting can be detected by monitoring one high-frequency measurement in the capacitive region and one low-frequency measurement in the dc impedance region. Alternatively, the dc impedance can also be calculated using dc operating point measurements. The proposed hot-spot detection method can be integrated into a dc–dc power converter that operates at the panel or subpanel level.

Index Terms—Fault detection, impedance measurement, photovoltaic (PV) hot spot, partial shading, PV systems.

Manuscript received October 24, 2014; revised January 10, 2015; accepted March 14, 2015. Date of publication March 30, 2015; date of current version September 29, 2015. This work was supported in part by the Grainger Center for Electric Machinery and Electromechanics at the University of Illinois at Urbana-Champaign, Seoul National University Power Electronics Center, the 1.140099.01 Research Fund at the Ulsan National Institute of Science and Technology (UNIST), U.S. National Science Foundation through the Graduate Research Fellowship Program, the Advanced Research Projects Agency-Energy (ARPA-E), U.S. Department of Energy, under Award DE-AR0000217, and by an agency of the United States Government. The information, data, or work presented herein was funded in part by an agency of the United States Government. Neither the United States Government nor any agency thereof, nor any of their employees, makes any warranty, express or implied, or assumes any legal liability or responsibility for the accuracy, completeness, or usefulness of any information, apparatus, product, or process disclosed, or represents that its use would not infringe privately owned rights. Reference herein to any specific commercial product, process, or service by trade name, trademark, manufacturer, or otherwise does not necessarily constitute or imply its endorsement, recommendation, or favoring by the United States Government or any agency thereof. The views and opinions of authors expressed herein do not necessarily state or reflect those of the United States Government or any agency thereof. This paper was presented in part at the *IEEE Applied Power Electronics Conference*, Long Beach, CA, USA, March 17–21, 2013. Recommended for publication by Associate Editor V. Agarwal.

K. A. Kim is with the School of Electrical and Computer Engineering, Ulsan National Institute of Science and Technology, Ulsan 689-798, South Korea (e-mail: kkim@unist.ac.kr).

G.-S. Seo and B.-H. Cho are with the Department of Electrical and Computer Engineering, Seoul National University, Seoul 151-744, South Korea (e-mail: gabzsu@snu.ac.kr; bhcho@snu.ac.kr).

P. T. Krein is with the Department of Electrical and Computer Engineering, University of Illinois at Urbana-Champaign, Urbana, IL 61801 USA (e-mail: krein@illinois.edu).

Color versions of one or more of the figures in this paper are available online at <http://ieeexplore.ieee.org>.

Digital Object Identifier 10.1109/TPEL.2015.2417548

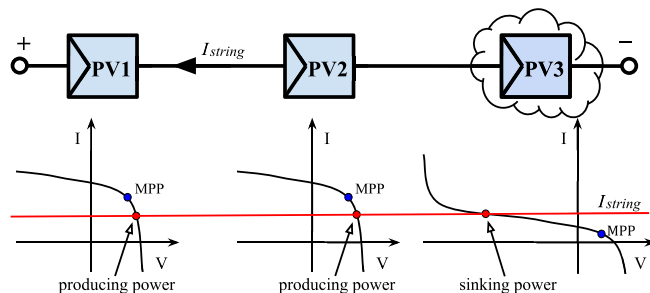


Fig. 1. Partially shaded string of PV cells showing reverse voltage bias of the shaded cell. Each cell's electrical characteristics are shown with the MPP and the operating point according to string current I_{string} .

I. INTRODUCTION

PHOTOVOLTAIC (PV) hot spotting is a temporary fault condition that occurs in series-connected PV cells. In most commercial PV panels, cells are strung in series to reach high output voltages required for many PV applications, such as grid-connected systems. Ideally, the electrical characteristics of all cells in the string are identical and the string operates at the maximum power point (MPP) current to achieve each cell's optimal output. However, when there is mismatch among the cell electrical characteristics, the single string current is unable to operate at every cell's MPP, which leads to suboptimal performance [1]. There are many factors that can create mismatch, such as manufacturing error tolerance, partial shading, and degradation.

When there are only a few underperforming cells (e.g., due to heavy shading) in a string of normal cells, the imposed string current tends to reverse bias the compromised cells. Fig. 1 illustrates a shaded cell becoming reverse biased in a PV cell string. PV1 and PV2 are under normal illumination, while PV3 is shaded. Shading the cell shifts the electrical characteristics down on the current axis, as shown in the I - V plot for PV3, such that the MPP current decreases. In this example, the string current (I_{string}) settles to a current that is greater than PV3's short-circuit current, causing its voltage to become reverse biased. Because voltage is negative but current is flowing, the shaded cell sinks power rather than sources power. If the cell sinks significant power, the generated heat drastically increases the localized cell temperature, which can damage the cell [2]; this is commonly known as hot spotting [1], [3].

For clarity, this paper defines *hot spotting* as a temperature increase of a PV cell or a portion of the cell above the temperature of its surroundings due to reverse-bias power dissipation. The term *hot spot* refers to the portion of the cell with a higher

temperature due to hot spotting. *Hot-spot damage* refers to permanent damage or degradation of a PV cell caused by hot spotting.

In early satellite systems, hot spotting was identified as a condition that could permanently damage PV cells [4]. A prevention method was developed, commonly called the *bypass diode*, which places a passive diode in parallel with the PV string in order to provide an alternate current path around the PV string when hot spotting occurs. A bypass diode or, more recently, an active bypass switch [5] placed over PV panel substrings is still the main prevention method for hot spotting today. Although bypass diodes and active bypass switches mitigate the hot spotting problem (i.e., limit the amount of power that can be dissipated through the PV cell) [6], they do not prevent hot spot damage. Field studies have shown that hot spotting is a major cause of panel performance degradation, even in systems employing bypass diodes [7]–[9]. Once a cell is degraded from hot spotting, it becomes a weak point in the string that causes performance reduction of the entire PV panel [10]. Hot spotting occurs more easily in a degraded cell, which exacerbates the hot-spot degradation problem.

Hot-spot damage could be avoided if bypass diodes are placed over a small enough number of cells because the potential reverse-bias power dissipation through a cell is proportional to the number of cells in the string [6]. Preliminary studies indicate that placing a bypass diode over every three cells (or fewer) would prevent hot-spot damage [11]. This approach would require bypass diodes integrated into the PV panel itself, rather than the junction box. In the past, some designers advocated bypass diodes across every cell [12], [13]. However, the operating requirements on these bypass diodes are extreme due to high currents, so incorporating a large numbers of power diodes has not been a practical solution. In general, mainstream Si PV panel manufacturers have not integrated additional electronics into the panel itself, likely due to increased construction cost and complexity.

Because panel manufacturers are reluctant to integrate components and electronics into the panel itself, this work focuses on hot-spot prevention at the subpanel-level, i.e., at the junction box level. The first part of this prevention method is the ability to detect if a cell within a subpanel string is hot spotting. A few hot-spot detection methods have been proposed previously, such as [14] and [15], which suggest methods that require sensor integration into the PV panel; these types of detection algorithms are unlikely to be adopted in the near future due to panel integration challenges and cost limitations. Additionally, a postmeasurement data processing detection method is proposed in [16] and a model-based hot-spot suppression algorithm is described in [17]. Both these methods have intensive processing requirements and significant additional hardware requirements, leading to high costs in the current market. This paper proposes a string-level hot-spot detection method that can be implemented using the existing dc–dc converter that controls the PV panel with minimal additional hardware and processing requirements. The detection algorithm utilizes PV string impedance measurements to detect hot spotting within a PV subpanel string. Preliminary work on the proposed hot-spot detection method was presented in [18]. This paper expands upon that work to provide a full

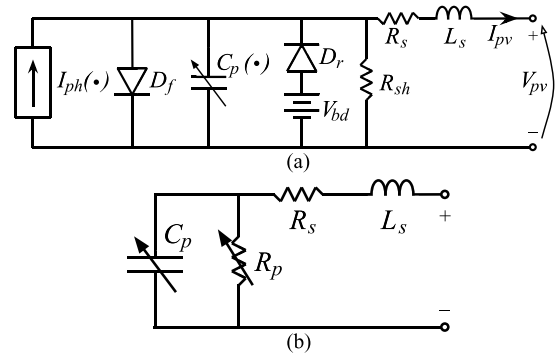


Fig. 2. Full (a) and ac small-signal (b) PV equivalent circuit model [19].

description of the hot-spot detection impedance measurement method with experimental validation.

II. PV CELL IMPEDANCE CHARACTERISTICS

The proposed hot-spot method is based on the change in PV impedance measurements during hot spotting. To understand the basic principle, the PV cell model is first examined and its impedance characteristics are analyzed over a range of frequencies. The characteristics are compared at various illumination conditions.

A. PV Cell Dynamic Model

A PV cell is essentially a p–n junction that can be modeled with associated resistance, capacitance, and inductance components, plus a photocurrent source that is proportional to illumination. The full PV equivalent circuit model with reverse-bias characteristics is represented by a model described in [19], which is shown in Fig. 2(a). For small-signal frequency analysis, the dc components (current source, voltage source, and diodes) are ignored, leaving the series resistance R_s , series inductance L_s , equivalent parallel resistance R_p , and equivalent parallel capacitance C_p . The ac small-signal PV equivalent circuit model is shown in Fig. 2(b). The equation for the equivalent circuit impedance at frequency ω is

$$Z = R_s + \frac{R_p}{(\omega R_p C_p)^2 + 1} + j \left[L_s \omega - \frac{\omega R_p^2 C_p}{(\omega R_p C_p)^2 + 1} \right]. \quad (1)$$

PV ac impedance characteristics can be represented in Bode plot form, as shown in Fig. 3. Each circuit parameter of the model can be linked to a region in the Bode plot. At low frequencies, the resistance sum, $R_s + R_p$, dominates and the impedance angle is zero. At mid-range frequencies, C_p dominates such that the impedance magnitude begins to decrease with frequency and the angle shifts toward -90° . At the resonance frequency, the magnitude is approximately R_s and the phase angle passes through zero. At high frequencies, L_s dominates such that impedance magnitude increases with frequency and the angle moves toward 90° .

It is assumed that the values of R_s and L_s are relatively constant. However, the values of the C_p and R_p model parameters vary depending on factors such as illumination, temperature, and cell voltage bias [20], [21]. When the R_p value changes,

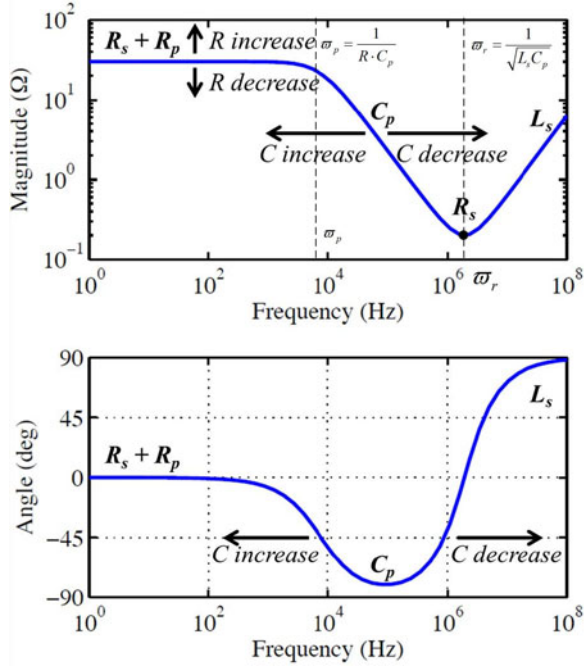


Fig. 3. Impedance Bode plot showing where the curve relates to the ac parameter values and how the curve changes as R and C change.

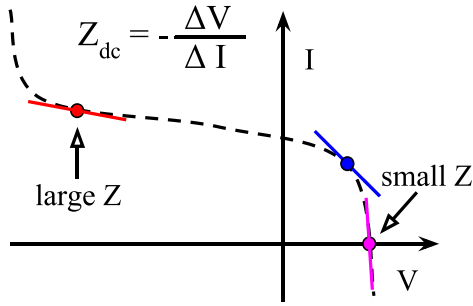


Fig. 4. PV cell I - V curve illustrating the dc impedance (Z_{dc}) based on the slope of the curve.

resistance changes are visualized as the resistive magnitude regions moving up or down directly with the resistance change. Changes in C_p are visualized as the capacitive magnitude region shifting left and right: left for C_p increase and right for C_p decrease. The phase dips in the frequency region where C_p dominates, and generally, shifts left (increasing C_p) and right (decreasing C_p) with capacitance, but its shape is also affected by the L_s and resistance values. The effects of these parameter changes are also shown in Fig. 3.

B. Parallel Resistance

For the proposed hot-spot detection method, the R_p value will need to be measured and monitored. The R_p value can be determined directly from the dc impedance, $R_p + R_s$, since it is assumed that R_s is constant. Generally, temperature increase slightly lowers resistance due to a higher number of free carriers, and increasing illumination also lowers resistance slightly [21], [22]. An intuitive way to understand how the dc impedance, and in turn, R_p change under various conditions is from the slope of

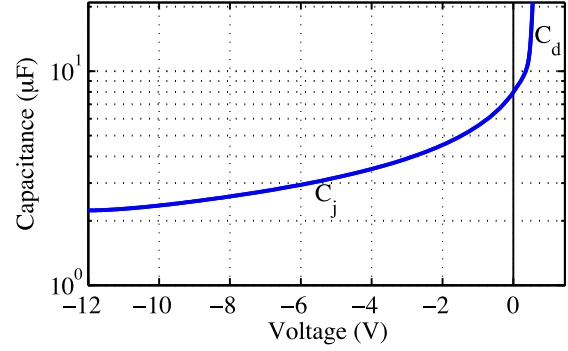


Fig. 5. PV cell parallel capacitance versus cell voltage, showing where junction capacitance (C_j) and diffusion capacitance (C_d) dominate.

the I - V curve. The equivalent dc impedance, Z_{dc} , is the negative change in voltage divided by the change in current as a result of a small perturbation, which is related to the slope of the I - V curve. An example I - V curve illustrating the dc impedance at various operating points is shown in Fig. 4. In regions where the slope is steep (reverse breakdown and above the MPP voltage), Z is small; in the middle horizontal region, Z is large.

C. Parallel Capacitance

The C_p value is also measured and monitored for the proposed hot-spot detection method. PV cell capacitance comes from two main sources: transition or junction capacitance (C_j) and diffusion capacitance (C_d). Junction capacitance, C_j , comes from the charge stored in the depletion region at the semiconductor p-n junction; it dominates at small positive and negative voltages, where the junction is not conducting significant current. Diffusion capacitance, C_d , comes from the charge stored in the neutral region of the semiconductor outside the depletion region. The diffusion capacitance is prominent when the p-n junction is forward biased above the MPP voltage, where the junction carries significant current, but it is negligible when reverse biased [21]–[23]. Fig. 5 illustrates capacitance trends over cell voltage bias and identifies the region where each capacitance type dominates. Generally, PV capacitance tends to increase with voltage bias, increase with temperature, and increase with illumination [21], [22].

III. AC MODEL PARAMETER CHARACTERIZATION

A. Experimental Setup

Experiments were conducted on a prototype PV panel with 18 Si cells in series. To access a single cell, panel material was cut away from one cell and wires are connected at each cell terminal. Halogen lights acted as the illumination source and were powered by a dc source to avoid ripple at the grid frequency. The Tenmars TM-207 solar power meter was used to measure light intensity at the panel surface. Temperature was measured at the back surface of the panel using the Minolta HT-11 spot thermometer. The Zahner Elektrik IM6ex impedance spectrum analyzer was used to take impedance measurements; tests utilize the potentiostat function. The spectrum analyzer had the capability to take impedance measurements while sinking

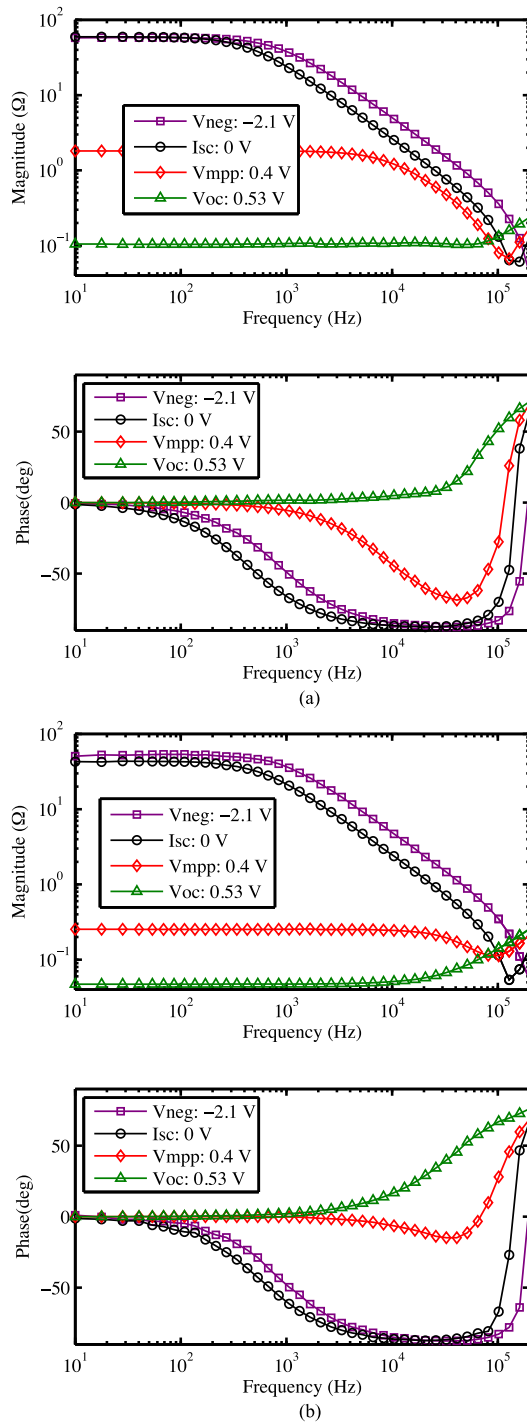


Fig. 6. Impedance plots for a PV cell at various voltage biases under (a) dark and (b) illuminated conditions.

or sourcing current up to ± 10 V and ± 2 A. Data were acquired using the Thales software provided by Zahner Elektrik.

B. Single PV Cell AC Parameters

A single PV cell was tested under dark conditions (no direct light) and under 1000-W/m^2 illumination over a range of -2.1 – 0.53 V. Tests were run after the module temperature stabilized at 30°C under dark and 50°C under illuminated conditions. Impedance plots for the cell under dark and illuminated condi-

TABLE I
PV CELL RESISTANCE AND CAPACITANCE VALUES

Voltage (V)	$R_s + R_p$ (Ω)		C_p (μF)	
	Dark	Illum.	Dark	Illum.
-2.10	58.2	52.2	3.24	3.30
0.0 (I_{SC})	59.7	43.1	6.31	6.71
0.40 (MPP)	1.81	0.253	10.2	306
0.53 (V_{OC})	0.104	0.0472	-	-

tions are shown in Fig. 6. The resistance and capacitance values calculated from the data are shown in Table I. Recall that the low-frequency flat region in the magnitude plot represents dc impedance ($R_s + R_p$) and the sloped region represents capacitance (C_p). For both lighting conditions, dc impedance decreases as voltage increases, indicating that R_p also decreases, and the sloped region moves to the left, indicating that capacitance increases.

These measurement plots verify two trends previously discussed in Section II: 1) as illumination and temperature increase, resistance decreases and capacitance increases and 2) as positive voltage bias increases, resistance decreases and capacitance increases. This is consistent with theory and findings in previous literature [20]–[23]. Based on data shown in Table I, changes in voltage bias tend to have a larger effect on the resistance and capacitance than illumination changes. The exception is at the 0.4-V MPP, where there is a significant jump in capacitance between dark and illuminated conditions; this is attributed to the significant increased temperature, which has a more significant effect on capacitance above the MPP. When temperature remains relatively constant, voltage bias has the biggest effect on the parallel resistance and capacitance values.

C. Series String AC Parameters

The full 18-cell string of PV cells was also tested under 1000-W/m^2 illumination with no shading, and then, with one cell covered by an opaque sheet to cause hot spotting in the shaded cell. Tests were run after the module temperature stabilized at approximately 47°C . Impedance plots under both conditions are shown in Fig. 7 and the calculated resistance and capacitance values are summarized in Table II. The unshaded case, shown in Fig. 7(a), is an extension of the single cell's characteristic. It shows the same trends: as voltage increases, parallel resistance decreases and capacitance increases. Fig. 7(b) shows the impedance plot for the partially shaded string exhibiting hot spotting. The change in the impedance characteristics depends on whether the string voltage is 0 V (short circuit), preshaded MPP voltage, or open-circuit voltage.

1) *Short Circuit (0 V)*: If the voltage is maintained at 0 V (short circuit), hot spotting caused by partial shading leads to resistance decrease and capacitance increase. In this experiment, the shaded cell had a negative bias of -8.5 V. Since the string voltage is 0 V, the remaining 17 cell voltages must sum to 8.5 V (0.5 V for each cell). After shading, the string dc impedance decreases, indicating that the reverse-biased cell is in its breakdown region, which has a lower dc impedance. For the capacitance

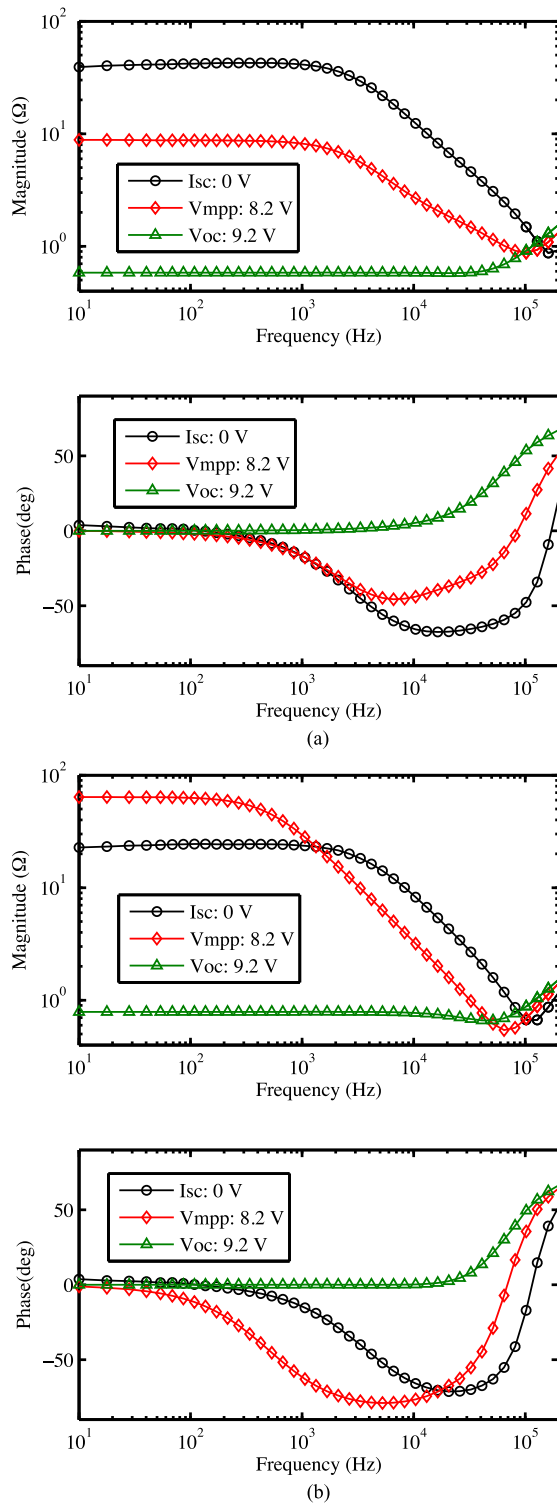


Fig. 7. Impedance plots for an (a) unshaded and a (b) shaded PV string.

value, the shaded cell decreases slightly in capacitance due to the negative voltage bias, while the positively biased unshaded cells increase in capacitance; the end result is a slight increase in string capacitance.

2) *Unshaded MPP*: If the voltage is maintained at the unshaded string's MPP of 8.2 V, partial shading results in a significant resistance increase and clear capacitance increase. In the experiment, the shaded cell becomes negatively biased at

TABLE II
PV STRING DC IMPEDANCE AND CAPACITANCE VALUES

Voltage (V)	$R_s + R_p$ (Ω)		C_p (μF)	
	Unshaded	Shaded	Unshaded	Shaded
0.0 (I_{SC})	40.3	23.4	1.126	1.86
8.2 (MPP)	8.81	63.9	4.72	5.48
9.2 (V_{OC})	0.583	0.787	-	634

−0.46 V, such that the remaining 17 cells increase in voltage bias (from 0.46 to 0.51 V). Overall, the string's equivalent resistance increases, indicating that the new operating point is in a flatter region of the I – V curve. The shaded cell's capacitance decreases, while unshaded cells' capacitance increases. The 17 unshaded cells' capacitance dominates and the overall string capacitance increases.

3) *Open-Circuit Voltage*: If the open-circuit voltage of 9.2 V is held constant, shading a cell results in a slight resistance increase; the capacitance value cannot be calculated because the wire inductance begins to dominate before the capacitance characteristic is observable. When the cell is shaded, its voltage decreases slightly (from 0.51 to 0.44 V), but remains positive. The overall string resistance increases, but only by 0.2 Ω . Based on the theory, the capacitance in the shaded cell is expected to decrease slightly and the unshaded cells are expected to increase such that the overall string capacitance increases.

D. AC Characteristics Under Maximum Power Point Tracking Control

During normal operation, a power converter controls the operation of the PV string, using a maximum power point tracking (MPPT) algorithm. Some algorithms maintain a relatively constant voltage throughout operation, such as fractional open-circuit voltage control, while other maximum-seeking algorithms continually track the MPP, e.g., perturb and observe (P&O) or ripple correlation control [24]–[26]. When the string is under constant voltage control near the unshaded MPP, Table II has already shown that there is a clear increase in resistance and capacitance. The Bode plots of the PV string before and after partial shading are compared in Fig. 8(a), which shows R_p and C_p increasing after hot spotting occurs.

Next, consider a maximum-seeking algorithm that adjusts the operating point to find the new MPP. One drawback of maximum-seeking algorithms is that they can sometimes operate at a local maximum rather than the true maximum. In the conducted experiment, the partially shaded string had a true MPP at 8.70 V and a local maximum at 8.05 V. Impedance measurements are taken at both maxima points and compared to the unshaded string measurement, as shown in Fig. 8(b). At both maxima points, there is a significant increase in resistance and a clear capacitance increase compared to the unshaded string.

Under either a constant-voltage or maximum-seeking type of MPPT control algorithm, hot spotting of one cell in an 18-cell string results in a clear dc impedance increase and capacitance increase. The dc impedance increase indicates that shading has caused the slope at the operating point to become more

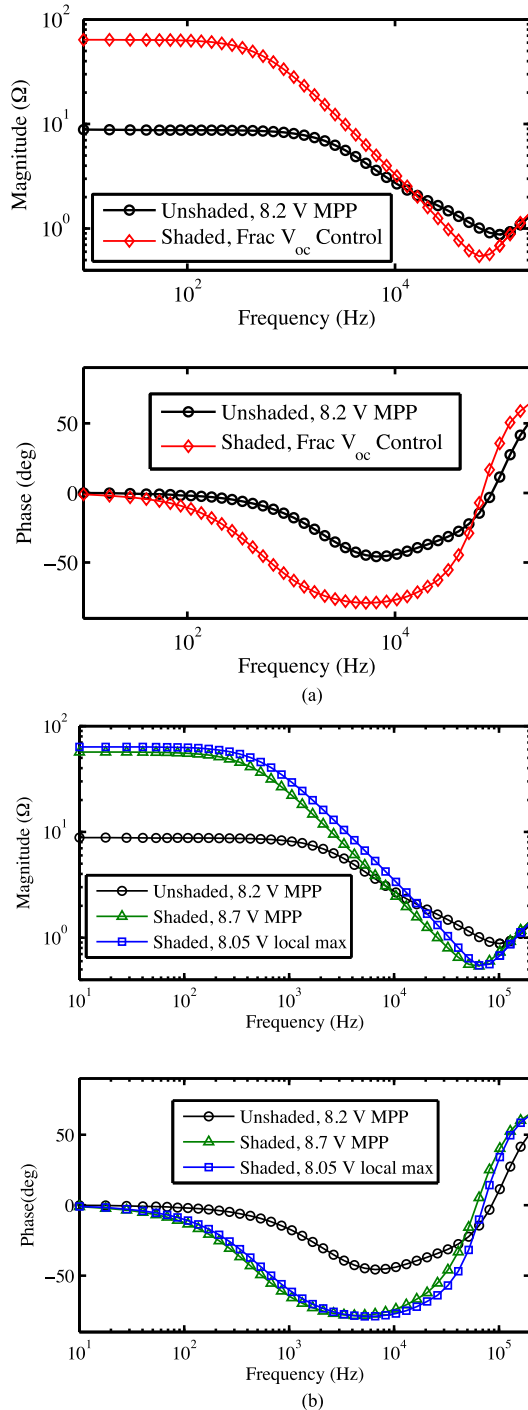


Fig. 8. String impedance plots before and after shading for fractional open-circuit voltage (a) and P&O (b) MPPT control.

shallow and that the shaded cell is moderately reverse biased. If the shaded cell operates in the reverse breakdown region, the operating point may have a steep slope resulting in a dc impedance decrease. DC impedance increase is possible; however, when the string is controlled with MPPT, the dc impedance tends to increase. Capacitance is expected to consistently increase when hot spotting occurs. These trends under hot spotting are consistent as long as the string maintains operating in the region near the MPP or a local maximum, which is true for most MPPT control algorithms.

The change in the dc impedance is best measured at lower frequencies. In the experimental results shown in Fig. 8, a frequency below 300 Hz can be used to measure the dc impedance. In this low-frequency range, an increase in the impedance magnitude indicates an increase in the PV string dc impedance. The change in capacitance is best measured at higher frequencies. Based on the experimental results in Fig. 8, a frequency range of approximately 10 to 70 kHz can be used to easily measure capacitance. In this frequency range, there is a clear decrease in the impedance magnitude under hot spotting, indicating a capacitance increase.

IV. HOT-SPOT DETECTION METHOD

Now that the changes in PV string characteristics under hot spotting have been established, the next step is to develop a detection algorithm. Here, a two-frequency measurement technique that can be used to monitor capacitance and dc impedance is proposed. In addition, an alternative method is also proposed to monitor dc impedance. The detection methods are validated with experimental results.

A. Two-Frequency Measurement Technique

The previous Bode plots included measurements over a wide range of frequencies but not all frequencies are needed to detect changes in capacitance and resistance. Each frequency measurements requires additional time and processing power. An effective detection system would use the fewest possible frequency measurements that still allow for accurate hot spot detection. Since dc impedance can be measured at low frequencies and capacitance can be measured at higher frequencies, a hot-spot detection method that uses one frequency measurement for each frequency range is investigated, referred to here as the two-frequency measurement technique. A low frequency, below approximately 300 Hz, is used to detect the equivalent resistive value of the string. For this experiment, 50 Hz is chosen to measure dc impedance because it is a low frequency where the impedance measurements is very clear without being an extremely low frequency. A higher frequency, between 10 and 70 kHz, is used to detect the equivalent capacitance of the string. For this experiment, 50 kHz is chosen to measure capacitance because experimental results show a large impedance magnitude change at this frequency.

1) *Experimental Setup*: In this experiment, a string of 24 multicrystalline Si cells were strung in series to represent a substring within a typical commercial panel. At each frequency, the impedance value was examined over a range of string voltage biases. An automated test was designed using the HP 33120A function generator to create the ac signal, Keithley 2420 to create dc offset, and Tektronix MSO4034 oscilloscope to measure and record the output signals. The halogen light illumination level was approximately 500 W/m².

2) *Capacitance Measurement at 50 kHz*: A 50-kHz sine waveform is used to measure the impedance of the PV string over a range of positive and negative operating voltages, for both the unshaded and one-cell shaded conditions. The string's 50 kHz impedance magnitude measurement is shown in Fig. 9(a) along with the calculated capacitance value in Fig. 9(b) for the

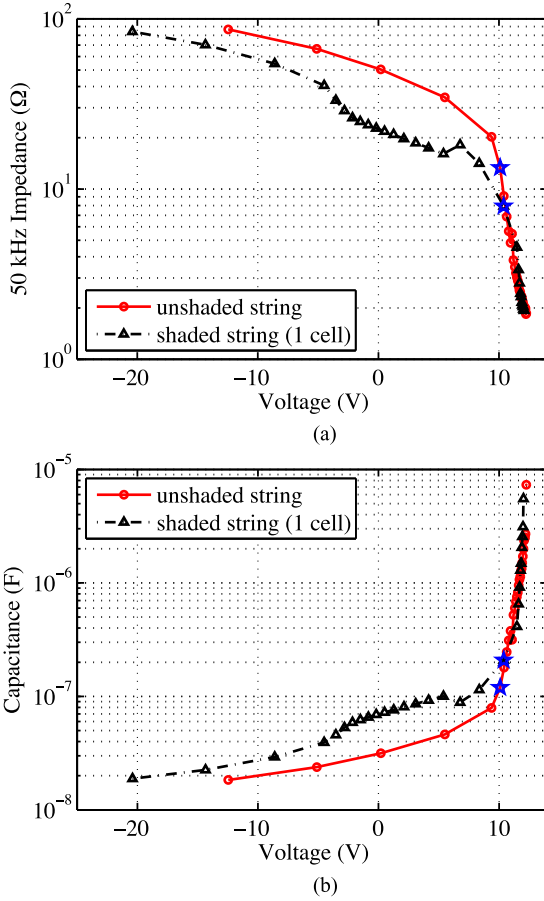


Fig. 9. Impedance measurements at (a) 50 kHz and (b) calculated capacitance for a 24-cell string unshaded at 500 W/m^2 , and then, with one cell shaded.

unshaded and shaded conditions. The MPP of each condition is marked with a star. As shown, there is a clear impedance decrease (capacitance increase) for voltages at and below the MPP voltage, where the string is expected to operate. These results verify that measuring the PV string impedance magnitude at one frequency can detect the characteristic changes that result from hot spotting.

As long as the frequency is in the range where the impedance magnitude decreases under hot spotting conditions, which is approximately 10–70 kHz for the results shown in Fig. 8, then the single frequency measurement should properly detect the capacitance change. Ideally, the frequency should be chosen such that hot spotting results in the largest impedance magnitude decrease for ease of detection, but any value within the measurement range will decrease under hot spotting conditions. In implementation, the switching frequency of the dc–dc converter that controls the PV substring could be set to the desired frequency to monitor the string capacitance.

B. Resistance Measurement at 50 Hz

A 50-Hz sine waveform is used to measure the PV string impedance over a range of positive and negative operating voltages. The string's I – V curve is shown in Fig. 10(a) and the 50-Hz impedance magnitude measurements in Fig. 10(b) for the un-

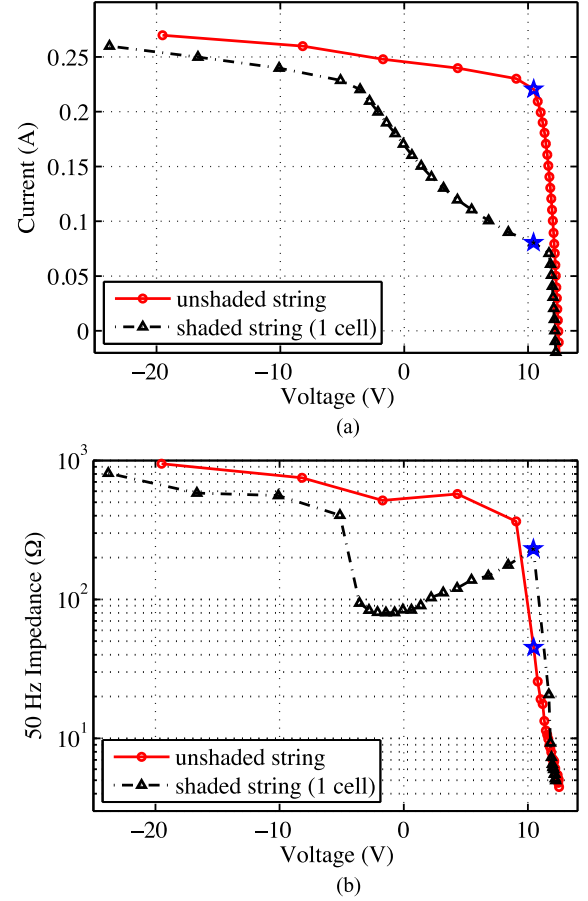


Fig. 10. I – V curve measurements (a) and impedance at 50 Hz (b) for a 24-cell string unshaded at 500 W/m^2 , and then, with one cell shaded.

shaded and shaded cases. The MPP for each case is, again, marked with a star. The impedance value correlates well with the slope of the I – V curve as discussed in Section II-B. After hot spotting has occurred, the string is most likely to operate at a voltage lower than the MPP voltage, under most MPPT algorithms. As shown in Fig. 10(b), an impedance increase is observed for the string. These results verify that changes in dc impedance due to hot spotting can be monitored using measurements at one low-frequency value. The source of such a 50-Hz signal that can be used for this measurement is less obvious. A low-frequency signal could potentially be derived from the 60-Hz (or 50-Hz) grid frequency but may require additional hardware, such as a small transformer. Alternatively, a digital controller could be programmed to create a perturbation at the desired frequency. These potential implementation techniques will be explored in future work.

C. I – V Curve Measurement Method

An alternative dc impedance method is also proposed that does not require a low-frequency perturbation signal. This I – V curve measurement technique utilizes the basic concept that the slope of the I – V curve at the operating point is equivalent to the dc impedance value ($R_s + R_p$). Some MPPT algorithms, such as P&O, continue to take small steps above and below the MPP

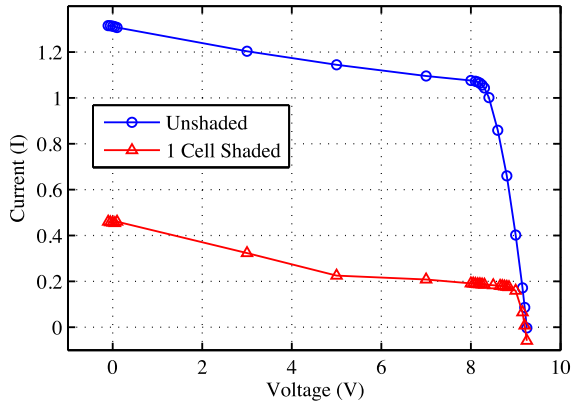


Fig. 11. Unshaded and shaded solar cell string I - V characteristics.

TABLE III
DC RESISTANCE ESTIMATES AND MEASUREMENTS FOR A PARTIALLY SHADED STRING

String State	Operat. Point	Volt. (V)	$R_s + R_p$ Meas. (Ω)	Curve Calc. (Ω)	Err. (%)
unshad.	V _{mpp}	8.2	8.79	8.13	-8
	V _{mpp}	8.7	56.8	47.6	-16
shaded	unshad. V _{mpp}	8.2	63.8	69.0	8
	local V _{mpp}	8.1	63.5	45.5	-28

under steady-state operation. The dc resistance at the operating point can be estimated from the measured I - V points around the MPP. This concept is tested on the PV string under unshaded and shaded conditions. The dc resistance values measured with the impedance spectrum analyzer are compared to the value estimated from the I - V curve. Fig. 11 shows the unshaded and shaded string I - V characteristics, from which the dc resistance is estimated. At each operating point, the current and voltage is measured above and below the point by a voltage step of 0.05 V. The impedance value is calculated from the linear slope from the two points above and below the operating point. Table III compares the measured and estimated dc resistance value for both the unshaded and partially shaded string conditions. The error magnitude is up to 28%, but the error could be decreased with higher current measurement resolution and a smaller voltage step size. These results confirm that a control method that measures the I - V characteristics around the operating point can estimate the dc resistance with enough accuracy to detect a clear change in the dc impedance value.

D. Discussion

1) *Various String Lengths:* Results presented previously in this paper showed that dc impedance and capacitance increase under hot spotting for two different strings of 18 and 24 Si PV cells. Typical PV subpanel strings vary from 12 to 36 cells in series. A preliminary simulation study was conducted to examine if the same trends hold true for these string lengths. A crystalline PV cell was modeled as in [19], and then, simulated under uniform 1000 W/m^2 irradiance, and then, with one cell shaded at

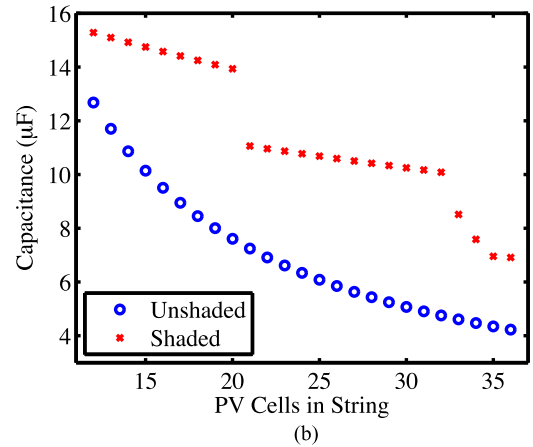
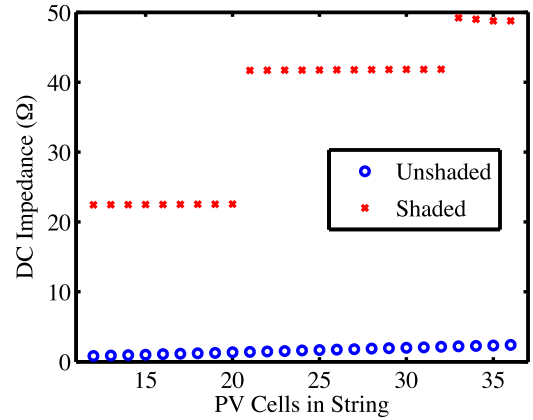


Fig. 12. Changes in string MPP (a) dc impedance and (b) capacitance under unshaded and shaded (hot spotting) conditions for various string lengths.

50 W/m^2 to induce hot spotting. Under both unshaded and shaded conditions, the string MPP is found and the dc impedance and capacitance values are compared. The results for strings of 12 to 36 cells in series are shown in Fig. 12. The dc impedance, shown in Fig. 12(a), shows a consistent increase under the hot-spotting condition. The capacitance, shown in Fig. 12(b), also shows a consistent increase. This indicates that the same trends are expected for a range of typical string lengths and that the proposed detection method is expected to work for most commercial crystalline Si PV substrings. However, these results also indicate that the impedance magnitude change expected due to hot spotting may vary depending on string length. The hot-spot detection algorithm will have to be calibrated for specific factors of the PV string, such as number of cells. A more extensive study into the effect of string length on the detection algorithm will be investigated in future work.

2) *Detection Method Considerations:* If a P&O MPPT method is used on the PV string, the I - V curve measurement method in combination with the high-frequency capacitance measurement may be the most appropriate hot spot detection method. The PV string voltage and current points are already measured to run the P&O algorithm, so only a simple calculation in the controller is required to estimate the dc impedance. The tradeoff is higher error, as shown in Table III. Also, a longer time

is required to estimate the value since a point above and below the steady-state MPP must be measured. Thus, the measurement would not be accurate during fast or frequent irradiance changes. If the string experiences irradiance changes in between P&O measurements, the estimated dc impedance would not be accurate. Alternatively, the low- and high-frequency measurement method is more accurate, but requires additional circuitry to generate the low-frequency signal or higher computing requirements to digitally generate the signal.

3) *Implementation*: The hot-spot detection method described utilizes only the impedance magnitude. As described in Section III, both the magnitude and phase of the characteristics change during hot spotting. Initially, only the magnitude is measured in order to reduce the number of required measurements. If there is a problem with false positives in the hot-spot detection method, then the phase could also be calculated to prevent false positives; however, this would increase computing requirements. This paper has fully described the basic hot-spot detection concept and validated its operation for typical sub-panel string lengths of Si PV cells. The next steps are to integrate the detection circuitry into a dc-dc converter and show that it can accurately detect hot spotting during normal MPPT operation. Further exploration into the best implementation method for this detection method is left as future work.

V. CONCLUSION

Hot spots form in series-connected PV cells, such as in a PV panel, under mismatched conditions among the PV cells. Hot spotting reduces string power and permanently degrades the hot-spot area within a PV cell. The present-day prevention method for hot-spot protection in PV panels is the bypass diode, but various studies have shown that (although it mitigates the problem) it does not prevent hot spotting or hot-spot damage. This paper has proposed a string-level hot-spot detection concept that measures changes in the string's small-signal impedance to identify hot spotting.

The PV cell model has been presented showing the effects of voltage bias, illumination, and temperature on model parameters. The small-signal model resistances (R_s and R_p) and capacitive (C_p) parameters are characterized for a single Si PV cell under dark and light conditions. Results show that changes in voltage bias have a larger effect on the resistance and capacitance values than changes in illumination. AC model parameters were also characterized for a PV subpanel string under uniform illumination conditions and hot-spotting conditions caused by partial shading. Experimental results showed that hot spotting within a string results in capacitance increase and dc impedance increase. These trends are consistent for both constant voltage and extremum-seeking MPPT control methods.

Hot-spot detection can be achieved with two frequency measurements: one for the higher frequency capacitive region and one for the low-frequency dc impedance region. Under hot-spotting conditions, experimental results on a 18-cell subpanel string show that measurements at 50 kHz and 50 Hz properly detect the changes in string capacitance and dc impedance, respectively. With certain MPPT algorithms, such as P&O, the low-

frequency measurement could be replaced with a method that estimates the dc impedance from the I - V curve measurements. Future work will further develop the hot-spot detection method and implement the algorithm using power converter hardware and control. The implementation of the proposed hot-spot detection concept will help increase PV lifetime power output by detecting and preventing hot spotting before it permanently damages the PV panel.

ACKNOWLEDGMENT

Neither the United States Government nor any agency thereof, nor any of their employees, makes any warranty, express or implied, or assumes any legal liability or responsibility for the accuracy, completeness, or usefulness of any information, apparatus, product, or process disclosed, or represents that its use would not infringe privately owned rights. Reference herein to any specific commercial product, process, or service by trade name, trademark, manufacturer, or otherwise does not necessarily constitute or imply its endorsement, recommendation, or favoring by the United States Government or any agency thereof. The views and opinions of authors expressed herein do not necessarily state or reflect those of the United States Government or any agency thereof.

REFERENCES

- [1] N. D. Kaushika and A. K. Rai, "An investigation of mismatch losses in solar photovoltaic cell networks," *Energy*, vol. 32, no. 5, pp. 755–759, May 2007.
- [2] D. Giaffreda, P. Magnone, M. Meneghini, M. Barbato, G. Meneghesso, E. Zanoni, E. Sangiorgi, and C. Fiegna, "Local shunting in multicrystalline silicon solar cells: Distributed electrical simulations and experiments," *IEEE J. Photovoltaics*, vol. 4, no. 1, pp. 40–47, Jan. 2014.
- [3] M. Alonso-Garcia, J. Ruiz, and F. Chenlo, "Experimental study of mismatch and shading effects in the I - V characteristic of a photovoltaic module," *Sol. Energy Mater. Sol. Cells*, vol. 90, no. 3, pp. 329–340, Feb. 2006.
- [4] E. Molenbroek, D. W. Waddington, and K. Emery, "Hot-spot susceptibility and testing of PV modules," in *Proc. IEEE Photovoltaic Spec. Conf.*, Oct. 1991, pp. 547–552.
- [5] G. Acciari, D. Graci, and A. L. Scala, "Higher PV module efficiency by a novel CBS bypass," *IEEE Trans. Power Electron.*, vol. 26, no. 5, pp. 1333–1336, May 2011.
- [6] K. A. Kim and P. T. Krein, "Photovoltaic hot spot analysis for cells with various reverse-bias characteristics through electrical and thermal simulation," in *Proc. IEEE Workshop Control Model. Power Electron.*, Jun. 2013, pp. 1–8.
- [7] C. Chamberlin, M. A. Rocheleau, M. W. Marshall, A. M. Reis, N. T. Coleman, and P. A. Lehman, "Comparison of PV module performance before and after 11 and 20 years of field exposure," in *Proc. IEEE Photovoltaic Spec. Conf.*, Jun. 2011, pp. 101–105.
- [8] P. Sanchez-Friera, M. Piliouge, J. Pelaez, J. Carretero, and M. S. de Cardona, "Analysis of degradation mechanisms of crystalline silicon PV modules after 12 years of operation in southern Europe," *Prog. Photovoltaics, Res. Appl.*, vol. 19, no. 6, pp. 658–666, 2011.
- [9] S. Kaplanis and E. Kaplani, "Energy performance and degradation over 20 years performance of BP c-Si PV modules," *Simul. Model. Practice Theory*, vol. 19, no. 4, pp. 1201–1211, 2011.
- [10] J. Sidawi, R. Habchi, N. Abboud, A. Jaafar, F. A. Allouch, G. E. H. Moussa, M. Aillerie, P. Petit, A. Zegaoui, and C. Salame, "The effect of reverse current on the dark properties of photovoltaic solar modules," *Energy Procedia*, vol. 6, pp. 743–749, 2011.
- [11] K. A. Kim and P. T. Krein, "Hot spotting and second breakdown effects on reverse I - V characteristics for mono-crystalline Si photovoltaics," in *Proc. IEEE Energy Convers. Congr. Expo.*, Sep. 2013, pp. 1007–1014.
- [12] C. H. Cox, D. J. Silversmith, and R. W. Mountain, "Reduction of photovoltaic cell reverse breakdown by a peripheral bypass diode," in *Proc. IEEE Photovoltaic Spec. Conf.*, 1982, pp. 834–839.

- [13] M. A. Green, E. S. Hasyim, S. R. Wenham, and M. R. Willison, "Silicon solar cells with integral bypass diodes," in *Proc. IEEE Photovoltaic Spec. Conf.*, 1984, pp. 513–516.
- [14] M. G. Real, U. Buhler, P. Toggweiler, G. Roth, and E. Bolliger, "Simplicity: From complex system design to standard product level," in *Proc. IEEE Photovoltaic Specialists Conf.*, Dec. 1994, vol. 1, pp. 716–721.
- [15] Y. Liu, B. Li, and Z. Cheng, "Research on PV module structure based on fault detection," in *Proc. Chinese Control Decision Conf.*, May 2010, pp. 3891–3895.
- [16] S. Ben-Menahem and S. C. Yang, "Online photovoltaic array hot-spot Bayesian diagnostics from streaming string-level electric data," in *Proc. IEEE Photovoltaic Spec. Conf.*, Jun. 2012, pp. 2432–2437.
- [17] S. A. Spanoche, J. D. Stewart, S. L. Hawley, and I. E. Opris, "Model-based method for partially shaded PV modules hot spot suppression," in *Proc. IEEE Photovoltaic Spec. Conf.*, Jun. 2012, pp. 1–7.
- [18] K. A. Kim, P. T. Krein, G.-S. Seo, and B.-H. Cho, "Photovoltaic ac parameter characterization for dynamic partial shading and hot spot detection," in *Proc. IEEE Appl. Power Electron. Conf.*, Mar. 2013, pp. 109–115.
- [19] K. A. Kim, C. Xu, J. Lei, and P. T. Krein, "Dynamic photovoltaic model incorporating capacitive and reverse-bias characteristics," *IEEE J. Photovoltaics*, vol. 3, no. 14, pp. 1334–1341, Oct. 2013.
- [20] D. Chenvidhya, K. Kirtikara, and C. Jivacate, "A new characterization method for solar cell dynamic impedance," *Sol. Energy Mater. Sol. Cells*, vol. 80, no. 4, pp. 459–464, Dec. 2003.
- [21] R. A. Kumar, M. S. Suresh, and J. Nagaraju, "Silicon (BSFR) solar cell ac parameters at different temperatures," *Sol. Energy Mater. Sol. Cells*, vol. 85, no. 3, pp. 397–406, Jan. 2005.
- [22] R. A. Kumar, M. S. Suresh, and J. Nagaraju, "GaAs/Ge solar cell ac parameters at different temperatures," *Sol. Energy Mater. Sol. Cells*, vol. 77, no. 2, pp. 145–153, May 2003.
- [23] R. A. Kumar, M. S. Suresh, and J. Nagaraju, "Measurement and comparison of ac parameters of silicon (BSR and BSFR) and gallium arsenide (GaAs/Ge) solar cells used in space applications," *Sol. Energy Mater. Sol. Cells*, vol. 60, no. 2, pp. 155–166, Jan. 2000.
- [24] T. Esmar and P. L. Chapman, "Comparison of photovoltaic array maximum power point tracking techniques," *IEEE Trans. Energy Convers.*, vol. 22, no. 2, pp. 439–449, Jun. 2007.
- [25] T. Esmar, J. Kimball, P. Krein, P. Chapman, and P. Midya, "Dynamic maximum power point tracking of photovoltaic arrays using ripple correlation control," *IEEE Trans. Power Electron.*, vol. 21, no. 5, pp. 1282–1291, Sep. 2006.
- [26] A. Bazzi and P. Krein, "Ripple correlation control: An extremum seeking control perspective for real-time optimization," *IEEE Trans. Power Electron.*, vol. 29, no. 2, pp. 988–995, Feb. 2014.



Katherine A. Kim (S'06–M'14) received the B.S. degree in electrical and computer engineering from Franklin W. Olin College of Engineering, Needham, MA, USA, in 2007, and the M.S. degree in electrical and computer engineering in 2011 and the Ph.D. degree in electrical and computer engineering in 2014, both from the University of Illinois, Urbana-Champaign, IL, USA.

She is currently an Assistant Professor of electrical and computer engineering at the Ulsan National Institute of Science and Technology, Ulsan, Korea,

and runs the Power Electronics for Advanced Renewable Systems Laboratory. Dr. Kim received the National Science Foundation's East Asia and Pacific Summer Institutes Fellowship in 2010 and Graduate Research Fellowship in 2011. She served as the Chair of the IEEE Power and Energy Society/Power Electronics Society Joint Student Chapter at the University of Illinois in 2010–2011 and the Codirector of the IEEE Power and Energy Conference at Illinois in 2012. She served as the Student Membership Chair for the IEEE Power Electronics Society from 2013 to 2014.



Gab-Su Seo (S'10) received the B.S. degree from Chonnam National University, Gwangju, Korea, in 2008, and the M.S. degree in electrical engineering from Seoul National University, Seoul, Korea, in 2010, where he is currently working toward the Ph.D. degree.

His research interests include design, analysis, and control of photovoltaic power conditioning systems, dc distribution systems, integrated resonant converters, and low-profile power supplies.

He is a student member of the IEEE Power Electronics Society and the IEEE Industrial Electronics Society.



Bo-Hyung Cho (M'89–SM'95–F'11) received the B.S. and M.S. degrees from the California Institute of Technology, Pasadena, CA, USA and the Ph.D. degree from Virginia Polytechnic Institute and State University (Virginia Tech), Blacksburg, VA, USA, all in electrical engineering.

Prior to his research at Virginia Tech, he was a member of the Technical Staff with the Department of Power Conversion Electronics, TRW Defense and Space System Group. From 1982 to 1995, he was a Professor in the Department of Electrical Engineering, Virginia Tech. In 1995, he joined the School of Electrical Engineering, Seoul National University, Seoul, Korea, where he is currently a Professor. His current research interests include power electronics, modeling, analysis, and control of spacecraft power processing equipment, and distributed power systems.

Dr. Cho received the 1989 Presidential Young Investigator Award from the National Science Foundation. He chaired the 2006 IEEE Power Electronics Specialists Conference. He is a member of Tau Beta Pi.



Philip T. Krein (S'76–M'82–SM'93–F'00) received the B.S. degree in electrical engineering and the A.B. degree in economics and business from Lafayette College, Easton, PA, USA, and the M.S. and Ph.D. degrees in electrical engineering from the University of Illinois at Urbana-Champaign, Champaign, IL, USA.

He was an Engineer with Tektronix, Beaverton, OR, USA, and then, returned to the University of Illinois at Urbana-Champaign. At present, he holds the Grainger Chair in Electric Machinery and Electromechanics and is a Professor and the Director of the Grainger Center for Electric Machinery and Electromechanics. His research interests include power electronics, machines, drives, and electrical energy, with emphasis on nonlinear control and distributed systems. He published an undergraduate textbook, *Elements of Power Electronics* (Oxford University Press, London, U.K., 2nd ed., 2014). In 2001, he helped initiate the International Future Energy Challenge, a major student competition involving fuel cell power conversion and energy efficiency. He holds 28 U.S. patents with additional patents pending.

Dr. Krein is a registered professional engineer in Illinois and in Oregon. He was a senior Fulbright Scholar at the University of Surrey in the United Kingdom in 1997–98, and was recognized as a University Scholar in 1999, the highest research award at the University of Illinois. He serves as Academic Advisor for the Department of Electronic and Information Engineering at Hong Kong Polytechnic University. In 2003, he received the IEEE William E. Newell Award in Power Electronics. He is a past President of the IEEE Power Electronics Society, and served as a member of the IEEE Board of Directors. In 2005–2007, he was a Distinguished Lecturer for the IEEE Power Electronics Society. In 2008, he received the Distinguished Service Award from the IEEE Power Electronics Society. He is Editor-At-Large of the IEEE TRANSACTIONS ON POWER ELECTRONICS and an Associate Editor of the IEEE JOURNAL OF EMERGING AND SELECTED TOPICS IN POWER ELECTRONICS. In 2015, he is serving as the Chair of the IEEE Transportation Electrification Community.